EPJ Web of Conferences **269**, 01024 (2022) https://doi.org/10.1051/epjconf/202226901024
EFM 2019

Pool boiling of ethanol on surfaces with parallel microchannels

Robert Kaniowski[1,*], *Robert* Pastuszko[1]

[1]Kielce University of Technology, Faculty of Mechatronics and Mechanical Engineering, al. 1000-lecia Państwa Polskiego 7, PL-25-314 Kielce, Poland

Abstract. The paper presents investigations into pool boiling heat transfer for open minichannel surfaces. The experiments were carried out with saturated ethanol at atmospheric pressure. Parallel microchannels fabricated by machining were about 0.2, 0.3 and 0.4 wide and 0.2 to 0.5 mm deep. The measurements were performed with increasing heat flux and variable geometric parameters of the minichannels. The image acquisition speed was 493 fps (at resolution 400 x 300 pixels with Photonfocus PHOT MV-D1024-160-CL camera) and an EX-FH20 (*Casio*) camera was used to record the images of the entire surface of the specimen. The analysis of boiling curves for the tested surfaces does not give an unambiguous response to the influence of geometrical parameters, i.e. the height of the microchannels on the heat transfer process.

1 Introduction

Modern technology needs compact heat exchangers, small in size but capable of removing high heat fluxes. High-performance miniaturised electronic systems necessitate finding ways of providing the most powerful cooling at smaller volumes and weight. Pool boiling is an attractive cooling technique that allows dissipating large amounts of heat flux at low superheats. Surface modification with microchannels in various shapes is a relatively simple method of pool boiling heat transfer enhancement.

Authors of [1,2] experimented with copper Ω-shaped samples having round cavities and narrow inlet directed upwards, with water and ethanol as boiling liquids at atmospheric pressure. The surface used highly increases the number of active nucleation sites, which makes it possible to remove large heat flux amounts at low superheats and high CHF. Visualization study showed bubble nucleation, growth and departure behaviours in reentrant cavities, and, at higher heat fluxes, the tendency of the bubbles to coalesce.

Kalani and Kandlikar in [3] used open microchannel structures to investigate the pool boiling performance of various geometric parameters (channel depth 245 – 470 μm, channel width 194 – 406 μm) with ethanol as the working fluid. Microchannels were machined over an area of 10 x 10 mm^2 in the middle of the 20 x 20 mm^2 test section. The authors concluded that the best performing chip had deep (400 μm) and narrow (200 μm) channels.

Studies on pool boiling heat transfer with water, ethanol, FC–72 and Novec-649 from tunnel structures, microfins, microchannels, microcavities [4–7] and boiling heat transfer with FC-72 flowing in narrow channels [8–10] have been conducted in order to determine the most favorable enhanced surfaces parameters in terms of the possibility of obtaining the highest heat transfer coefficients.

2 Experimental setup

The test set up [4-7], Figure 1 and Figure 2, is designed to determine boiling curves and to visually record the vapour bubble generation process. The heat transfer experiments on microfins were conducted for pool boiling in the range of nucleate boiling up to the boiling crisis. The level of liquid above the surface of the specimen was 50 mm. Prior to the measurements, ethanol was degassed by boiling for 15 minutes. Measurement data were recorded after all temperatures stabilized. The tests were performed at increasing heat flux up to the boiling crisis at atmospheric pressure.

The cylinder diameter corresponded to the diagonal of the sample base. A 1000 W electric cartridge heater 19 mm in diameter and 130 mm in length was mounted in a heating bar. Type *K* (NiCr-NiAl) sheathed thermocouples of 0.5 mm in diameter were used for the measurements. The measurement data acquisition system was a product of FLUKE Hydra 2635A. Calibration of the thermocouples was carried out using the Altek calibrator.

The images of the bubbles at the moment of their nucleation, growth and departure were obtained using a PHOT MV-D1024-160-CL (*Photonfocus*) digital monochromatic camera with a resolution of 1024x758 pixels. The camera recorded the photos at a speed of 493 fps at a resolution of 400x300 pixels, mean error 2 fps. An EX-FH20 (*Casio*) camera was used to record the images of the entire surface of the specimen. Lighting was provided by a halogen lamp with light pipes (front light and back light).

* Corresponding author: kaniowski@tu.kielce.pl

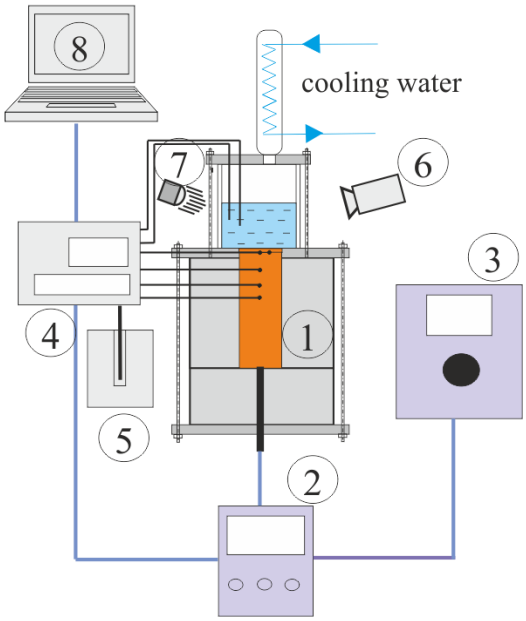

Fig. 1. Pool boiling measurement stand: 1 – main module, 2 – wattmeter, 3 – autotransformer, 4 – data logger, 5 – dry-well calibrator, 6 – high speed camera, 7 – light, 8 – PC.

Table 1. MC surface codes and specifications.

Sample code	*w* mm	*h* mm	*p* mm
Smooth surface	-	-	-
MC-0.2-0.5-0.4	0.2	0.5	0.4
MC-0.2-0.4-0.4	0.2	0.4	0.4
MC-0.2-0.3-0.4	0.2	0.3	0.4
MC-0.2-0.2-0.4	0.2	0.2	0.4
MC-0.3-0.5-0.6	0.3	0.5	0.6
MC-0.3-0.4-0.6	0.3	0.4	0.6
MC-0.3-0.3-0.6	0.3	0.3	0.6
MC-0.3-0.2-0.6	0.3	0.2	0.6
MC-0.4-0.5-0.8	0.4	0.5	0.8
MC-0.4-0.4-0.8	0.4	0.4	0.8
MC-0.4-0.3-0.8	0.4	0.3	0.8
MC-0.4-0.2-0.8	0.4	0.2	0.8

The specimens with test surfaces were made of copper and had parallel grooves with a constant pitch, made with an end mill of 0.2 – 0.4 mm in diameter (CNC machining process) and 0.2 to 0.5 mm deep. The test section consisted of a 32 x 32 mm^2 square copper specimen with a 27 x 27 mm^2 boiling region. Table 1 compiles the surface codes, specifications according to Fig. 2.

By Newton's law of cooling, HTC is equal:

$$\alpha = \frac{q}{\Delta T}, \tag{1}$$

According to Fourier's law:

$$q = \lambda_{Cu} \frac{dT}{dX} \cdot \frac{\pi d_c^2}{4a^2}, \tag{2}$$

The temperature gradient was calculated using three point's backward finite difference method as given below, Fig. 3.

$$\frac{dT}{dX} = \frac{3\frac{T_{T3}+T_{T4}}{2} - 4T_{T6} + T_{T7}}{2l_{T7-T3}}, \tag{3}$$

T_w was extrapolated by following equation as:

$$T_w = \frac{T_{T3}+T_{T4}}{2} - q\left(\frac{\delta_s}{\lambda_{Cu}} + \frac{\delta_{Sn}}{\lambda_{Sn}}\right), \tag{4}$$

where δ_s is distance between microchannel bottom (base) and thermocouples *T3* and *T4*.

The difference between temperatures of the heated surface and liquid ΔT (superheat) is shown by the following equation:

$$\Delta T = T_w - \frac{T_{T1}+T_{T2}}{2}, \tag{5}$$

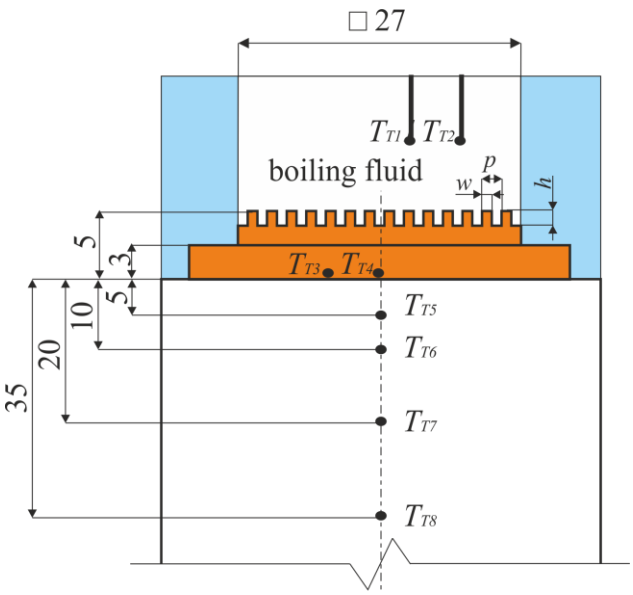

Fig. 2. Arrangemet of thermocouples.

3 Results

The investigated surfaces with open microchannels provided higher heat transfer coefficients compared to smooth surfaces. For the tested samples with microchannels, Table 1, a significant intensification of heat flux was observed, with the heat transfer coefficient depending on the depth and width of the microchannels. The best results were obtained for sample MC-0.2-0.5-0.4, where the maximum heat transfer coefficient was 56 kW/m^{2}K at superheat ΔT ~ 18.5 K, and heat flux about 1035 kW/m^2, Fig. 3a.

Analyzed surfaces with microchannels allow to obtain heat transfer coefficients within the range of 3.4 – 56 kW/m^2, which in relation to the flat, plain surface gives a 2-fold increase in HTC. The intensification of heat transfer for samples with

microchannels is demonstrated by the ratio of the heat transfer coefficient for the extended surface to the coefficient for the smooth surface, Fig. 3b.

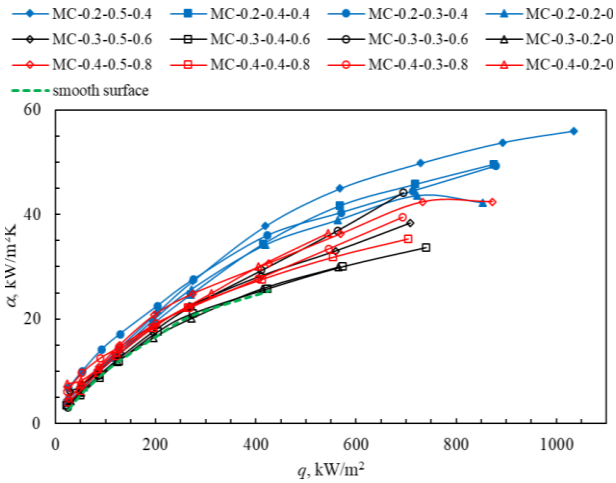

a)

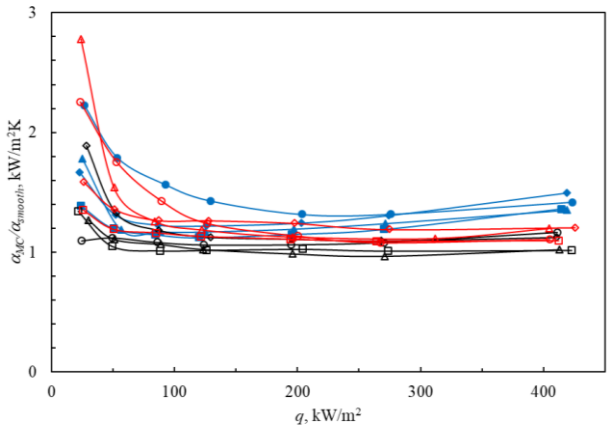

b)

Fig. 3. Boiling curves for ethanol, a) heat transfer coefficient vs. heat flux, b) data in the non-dimensional form for MC surfaces.

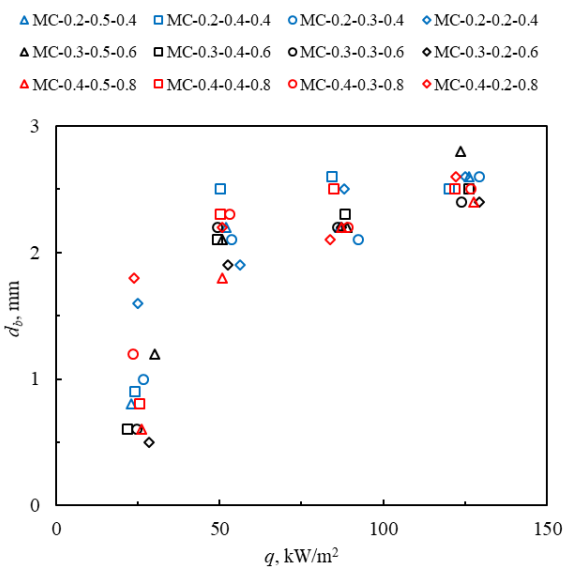

Fig. 4. Averaged departing bubble diameters for ethanol.

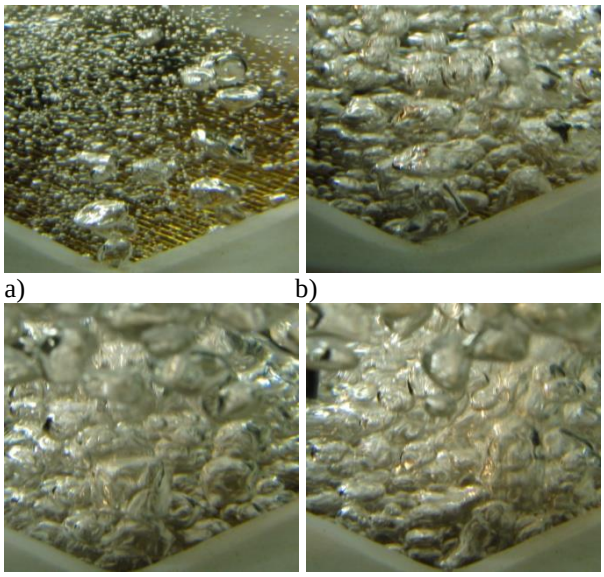

a) b)

c) d)

Fig. 5. Visualization observations of pool boiling of ethanol on microchannel surface MC-0.3-0.4-0.6. a) q = 21.9 kW/m^2, b) q = 49.3 kW/m^2, c) q = 88.2 kW/m^2, d) q = 126.2 kW/m^2.

Figure 4 presents the heat-flux-dependent averaged diameters of departing bubbles at boiling ethanol. Figure 5 shows bubble images on MFP surfaces for four different superheats. Vapor bubbles in microchannels generate in spaces between neighboring micro-fins, from where they move towards the fin tips, then grow and depart.

At small heat fluxes, relatively large distances between nucleation sites can be observed. At the same time, the detachable bubbles have a diameter slightly exceeding the width of the microchannel. As heat flux increases, the distances between the growing blisters decrease, and their diameters increase to 2.5 mm. It can be assumed that the initial intense increase in the diameter of the detachable blisters when increasing the heat flux from 20 to 50 kW/m^2 is associated with a simultaneous increase in the density of nucleation sites. On the other hand, setting the diameter of detaching bubbles at heat fluxes greater than 50 kW/m^2 will cause an intensive increase in the frequency of detaching bubbles.

Conclusion

The analysis of the graphs shows the following conclusions:

- The greatest HTC in the range of 3 – 56 kW/m^2 can be obtained using microchannels of width 0.2 mm and depth 0.5 mm.
- The small width is associated with a small pitch of microchannels, which in turn makes it possible to obtain the largest number of microchannels on the width of the sample.
- Above 800 kW/m^2, the analyzed surfaces with microchannels allow to obtain heat transfer coefficients in the range of 40 – 56 kW/m^{2}K.

- The critical heat flux at boiling ethanol for surfaces with best performance exceeds 1000 kW/m^2.
- An intense increase in the diameter of the departing bubbles was observed with an increase in heat flux in the range of 20 – 50 kW/m^2.

Nomenclature

a – specimen width, m,
CHF – critical heat flux,
d – diameter, m,
h – depth, m,
HTC – heat transfer coefficient,
l – distance between thermocouples, m,
MC – microchannel,
p – pitch, m,
q – heat flux, kW/m^2,
T – temperature, K,
w – width, m,

Greek symbols

α – heat transfer coefficient, W/(m^{2}K),
δ – thickness, mm,
λ – thermal conductivity, W/(mK),
ΔT – difference of temperature, K,

Subscripts

b – bubble,
c – cylinder,
Cu – copper,
s – sample,
Sn – tin,
w – wall.

References

1. D. Deng, J. Feng, Q. Huang, Y. Tang, Y. Lian, Int. J. Heat and Mass Transfer**, 99** (2016)
2. D. Deng, , W. Wan, J. Feng, Q. Huang, Y. Qin, Y. Xie, App. Therm. Ing. **107** (2016)
3. A. Kalani, S. G. Kandlikar, proc. ASME 10th Int. Conf. Nanochannels, Microchannels and Minichannels, Rio Grande, Puerto Rico (2004)
4. R. Kaniowski, R. Pastuszko, Ł. Nowakowski, EPJ Web of Conferences **14** (2017)
5. R. Kaniowski, R. Pastuszko, EPJ Web of Conferences **180** (2018)
6. R. Kaniowski, R. Pastuszko, EPJ Web of Conferences **18** (2018)
7. R. Pastuszko, Int. J. Therm. Sci. **125** (2018)
8. M. Piasecka, K. Strąk, Heat Transf. Eng. **40** (13-14) (2019)
9. K. Strąk, M. Piasecka, B. Maciejewska, Int. J. Heat Mass Transf. **117** (2018)
10. B. Maciejewska, K. Strąk, M. Piasecka, Int. J. Numerical Method for Heat & Fluid Flow **28** (1) (2018)